Double-Perovskite Interlayer Stabilized Highly Efficient Perovskite Solar Cells

Wenjun Xiang[1], Ethan Cronk[2], Jacob Wall[1], Kai Zhu[3], Joseph J. Berry[3, 4, 5], Liping Yu[2], Feng Yan[1]*

[1]School for Engineering of Matter, Transport, and Energy, Arizona State University, Tempe, 85287, USA
[2]Department of Physics and Astronomy, University of Maine, Orono, Maine, 04469, USA
[3]National Renewable Energy Laboratory, Golden, Colorado 80401, USA
[4]Renewable and Sustainable Energy Institute, University of Colorado Boulder, Boulder Colorado 80309 USA
[5]Department of Physics, University of Colorado Boulder, Boulder, Colorado 80309, USA

Abstract

Metal halide perovskite solar cells (PSCs) have emerged as a highly promising photovoltaic technology, boasting an impressive power conversion efficiency exceeding 26.1% and demonstrating cost-effective manufacturing. However, the long-term stability of these devices poses a significant challenge, hindering their widespread manufacturing and commercialization. To tackle the degradation issue inherent in perovskite solar cells, surface passivation techniques, particularly employing a thin layer of two-dimensional (2D) perovskites to create a 2D/3D heterostructure. Beyond this, the exploration of metal halide double perovskites adds a new dimension to the chemical and bandgap phase space of materials for optoelectronic applications. In this study, we leverage a wide bandgap double perovskite interlayer to enhance the stability of 3D metal halide perovskite. Specifically, the double perovskite nanoparticle $Cs_2AgBiBr_6$, with its substantial band gap of 2.2 eV and exceptional air stability, is utilized. Through optimization, a $Cs_2AgBiBr_6$-treated PSC achieves an open-circuit voltage of 1.12 V and an impressive power conversion efficiency of 19.52%. Additionally, the $Cs_2AgBiBr_6$ passivation layer proves effective in bolstering the stability of PSCs under ambient conditions. This work demonstrates an additional strategy and design motif to simultaneously boost the PCE of PSCs along with achieving improved stability.

Keywords: Double perovskite, Passivation layer, Single perovskite, Solar cells, Environmental stability

1. Introduction

*Corresponding author: fengyan@asu.edu

Organic-inorganic hybrid metal halide perovskite solar cells (PSCs) have attracted tremendous interest due to their superior optoelectronic properties, including strong light absorption, low exciton binding energy, long carrier transport lengths, relatively easy fabrication process, and low cost. [1-5] Recently, the power conversion efficiency (PCE) for single-junction PSCs has climbed to 26.1%. [6-8] Although it has remarkably improved PCE, the inherent drawbacks of PSCs such as its poor moisture stability, and limited thermal stability in operation, are stumbling blocks for its commercial utilization. [9, 10] The widely used solution fabrication process also often results in defects at grain boundaries and layer interfaces. Several groups have reported that photovoltage loss is one of the major shortcomings that limit the performance, which is related to the non-radiative recombination and charge transport at interfaces, particularly in ambient conditions. [11-13] Surface engineering, including surface passivation and additive introduction, has been devoted to suppressing the non-radiative recombination losses at interfaces. Inserting polymer layers, [14, 15] organic molecules, [16, 17] ionic liquids [18, 19], and two-dimensional (2D) materials [20-22] have demonstrated improved stability.

Double perovskites have attracted lots of attention in recent years due to their desired ambient stability. [23-25] As for solar cell application, although lots of double perovskites, such as $Cs_2AgBiBr_6$ exhibit high inherent stability, nevertheless, their wide and indirect band gap coupled with low charge carrier transport capability led to a low PCE of 2-6% for solar cells employing them. [26-28] The unique double perovskite structure with two different transition metals at the B site in the single ABX_3 perovskite halide structure, (where A is alkali-earth metal, B is the transition metal and X is the halides) has great ambient stability. [29, 30] As a result, double perovskite halides are attractive candidates to passivate the traditional three-dimensional single perovskite halide. [31] Particularly, compared to the widely used organic-inorganic halides 2D perovskites, inorganic double perovskite can also offer improved stability and the promise of amenability integration into the solar module manufacturing process. [32]

In this work, we employ the $Cs_2AgBiBr_6$ double perovskite as an interlayer to passivate the 3D perovskite, which improves the device stability. We first synthesize the $Cs_2AgBiBr_6$ nanopowders, which are stable in air and even in water, and then utilize a solution process to coat it on top of a single perovskite

($Cs_{0.05}FA_{0.85}MA_{0.15}PbI_{2.55}Br_{0.45}$) surface. For the champion device with the structure Glass/ITO/SnO_2/Perovskite/$Cs_2AgBiBr_6$/Spiro-OMeTAD/Au, we achieved a of 1.12 V, with a of 23.48 mA/cm^2, an FF of 74.36%, and a PCE of 19.52%. The protective effect of the double perovskite layer can contribute to the improved stability of the perovskite solar cell with $Cs_2AgBiBr_6$ for the device without any encapsulation.

2. Experimental Procedure

Materials

PbI_2 (Sigma-Aldrich, 99.999%), $PbBr_2$ (TCI America), formamidinium iodide (FAI, 99.99%, GreatCell Solar), methylammonium bromide (MABr, 99.99%, GreatCell Solar), CsI (99.9%, BeanTown Chemical), CsBr (99.9%, BeanTown Chemical), AgBr (99.995%, BeanTown Chemical), $BiBr_3$ (99%, BeanTown Chemical), Spiro-OMeTAD (99.87%, luminescence technology corp), $SnCl_2.2H_2O$ (97%, Acros Organics), thiourea (99%, Alfa Aesar), dimethyl sulfoxide (DMSO, 99.8%, Sigma-Aldrich), dimethyl formamide (DMF, 9.8%, Sigma-Aldrich), diethyl ether (anhydrous, 99.7%, Sigma-Aldrich), HBr (47.0-49.0%, BeanTown Chemical), Li bis(trifluoromethanesulfonyl)imide (Li-TFSI, 99.95%, Sigma-Aldrich), 4-tert-butylpyridine (TBP, 96%, Aladdin), chlorobenzene (anhydrous, 99.8%, Sigma-Aldrich) were used as received without any further purification.

Synthesis of $Cs_2AgBiBr_6$ powder

Solid CsBr (1.278 g), AgBr (1.347 g), and $BiBr_3$ (0.564 g) were dissolved in 30 mL HBr (47.0-49.0% in water) and reacted at 110 °C with stirring for 2h. The solution was cooled to room temperature overnight. Orange $Cs_2AgBiBr_6$ powder was obtained by centrifugation and evaporation.

Device Fabrication

The $Cs_{0.04}FA_{0.81}MA_{0.15}PbI_{2.55}Br_{0.45}$ perovskite precursor solution was prepared with corresponding molar ratios of PbI_2 (1.15 M), $PbBr_2$ (0.2 M), FAI (1.05 M), MABr (0.2 M), and CsI (0.05M) dissolved in a mixed solvent of DMF and DMSO with a volume ratio of 4:1. The prepared perovskite precursor was then stirred

at 65 °C. The hole transport layer (HTL) precursor was prepared by dissolving 73 mg of Spiro-OMeTAD in 1 ml of chlorobenzene mixed with 17.5 I and 33.6 I of bis(trifluoromethylsulfonyl)imide lithium salt and 4-tert-butylpyridine, respectively. $Cs_2AgBiBr_6$ powder was dispersed in isopropanol with ultrasonic treatment for 0-5mg/ml.

ITO substrates were cleaned by sonication with detergent solution, deionized water (DIW), acetone, and isopropanol, followed by a UV-ozone treatment for 30 min. The SnO_2 QDs were synthesized at room temperature. A 0.15 M solution of $SnCl_2.2H_2O$ in DIW with the presence of thiourea (CH_4N_2S) as a reaction accelerator was prepared and filtered with a 0.45 I PTFE filter. [33] The SnO_2 layer was then deposited by spin-coating followed by 1h annealing at 180 °C in ambient. The as-prepared substrates were treated with UV-ozone for 10 min and transferred into a nitrogen-filled glovebox. The single triple cation perovskite layer with 1.4M $Cs_{0.05}FA_{0.81}MA_{0.14}PbI_{2.55}Br_{0.45}$ (CsFAMAPbIBr) was deposited at 1000 rpm for 10 s and then 6000 rpm for 30 s. Diethyl ether (DEE) antisolvent was dropped on the spinning ITOs during the high-speed rotation 5 s before the end of the spin coating. The deposited films were then annealed at 100 °C for 55 min. To fabricate the $Cs_2AgBiBr_6$ layer, various $Cs_2AgBiBr_6$ solutions (i.e., 0 to 5mg/ml) were deposited onto the perovskite film by spin-coating at 3000 rpm for 30 s and then heated at 100 °C for 5 min. As an HTL layer, the Spiro-OMeTAD precursor solution was spin-coated at 3000 rpm for 30 s on top of the double perovskite layer. Finally, a 100 nm thick gold layer was evaporated on the HTL as an electrode layer.

Materials and Device Characterization

The surface morphology of synthesized $Cs_2AgBiBr_6$ powder was characterized by transmission electron microscopy (TEM, FEI Tecnai). X-ray powder diffraction (XRD) using 45 kV, 40 mA Cu K radiation was used to measure the crystal structures of $Cs_2AgBiBr_6$ powder and perovskite films. The surface morphology of the perovskite film and the cross-sectional images of the PSCs were characterized by scanning electron microscopy (SEM, Thermo Scientific Apreo). Surface composition was measured by X-ray photoelectron spectroscopy (XPS) using an Al-K source and hemispherical analyzer (SPECS). The electrical

characteristics were obtained using a solar simulator (Newport, Oriel Class AAA 94063A, 1000-Watt Xenon light source) with a Keithley 2420 source meter under simulated AM 1.5G (100 mW/cm^2) solar irradiation. The light intensity was calibrated using a silicon reference cell (Newport, 91150V, certified by National Renewable Energy Lab). The masked active area is 0.07 cm^2. The external quantum efficiency (EQE) was obtained by an EnliTech QE measurement system.

3. Results and Discussion

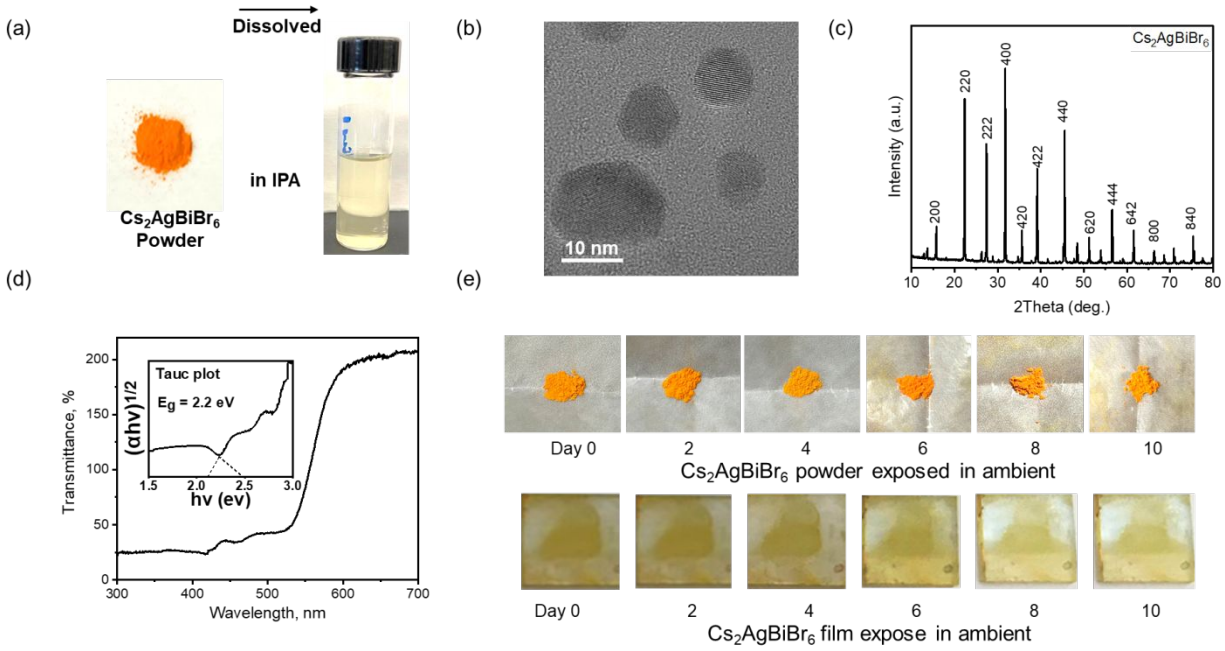

Figure 1. (a) $Cs_2AgBiBr_6$ powder and solution. (b) HRTEM image of $Cs_2AgBiBr_6$ nanoparticles. (c) XRD pattern (d) UV-vis image of $Cs_2AgBiBr_6$ nanoparticles (Insert: Tauc plot), and (e) the $Cs_2AgBiBr_6$ powder and film exposed to ambient with moisture RH~60% for various days.

Double perovskite $Cs_2AgBiBr_6$ powder was synthesized according to the method reported before. [27] Briefly, solid CsBr, AgBr, and $BiBr_3$ were dissolved in HBr (48% in water) and reacted at 110 °C with stirring for 2h. The synthesized $Cs_2AgBiBr_6$ powder shows orange color, as shown in Fig. 1a. The $Cs_2AgBiBr_6$ powder was then dissolved in isopropanol (IPA) at a concentration of 0 to 5 mg/ml to form a transparent light-yellow solution (Fig.1a) followed by ultrasonication and centrifuge process. As shown in Fig.1b, the

synthesized $Cs_2AgBiBr_6$ nanoparticles have a typical particle size of about 10 nm on average, which could provide a uniform coverage on the surface of the perovskite absorber layer. The $Cs_2AgBiBr_6$ solution was deposited on ITO/SnO_2 and characterized by X-ray diffraction (XRD) for the crystalline structure (Fig. 1c). The indexed diffraction planes of $Cs_2AgBiBr_6$ nanoparticles show the expected well-defined polycrystalline face-centered cubic structure phase (Fm3m). [28, 34] A strong absorption peak was observed using Ultraviolet-visible transmittance spectra (UV-vis) as shown in Fig. 1d for $Cs_2AgBiBr_6$, which is attributed to the indirect bandgap ~ 2.2eV as determined by the Tauc plots equation. The $Cs_2AgBiBr_6$ is stable in the ambient with RH~60% in both powder and film states as shown in Fig. 1e.

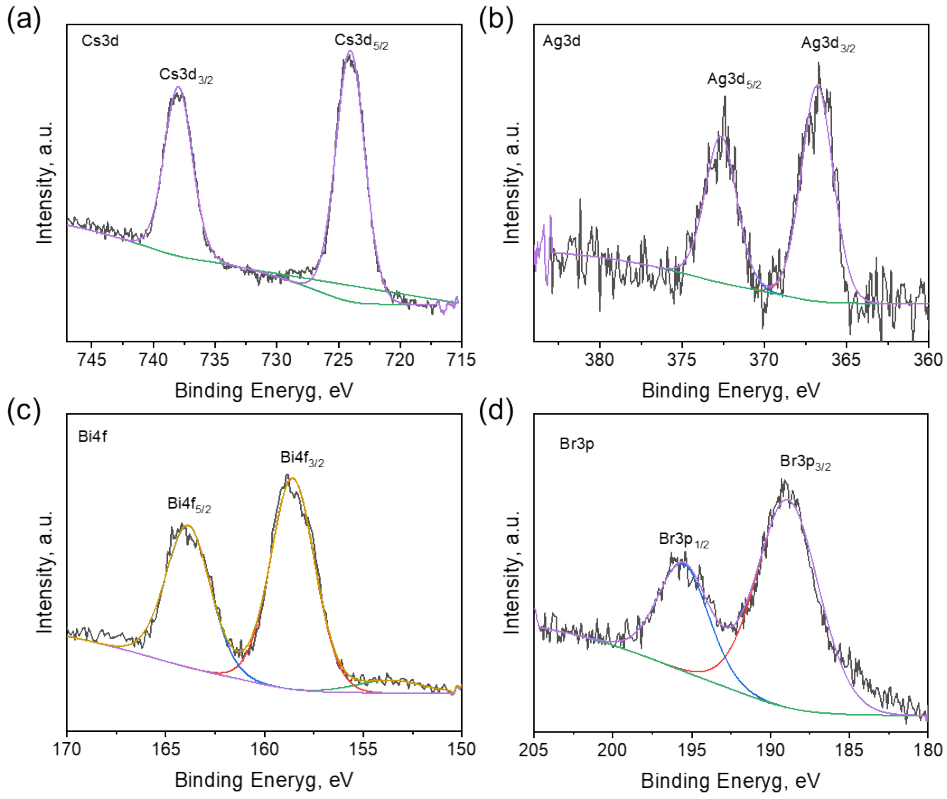

Figure.2 XPS scans of (a) Cs3d, (b) Ag3d, (c) Bi4f, and (d) Br3p core level of $Cs_2AgBiBr_6$ thin film.

To determine the chemical composition of the synthesized $Cs_2AgBiBr_6$ powders, X-ray photoelectron spectroscopy (XPS) has been conducted as shown in Fig. 2. The XPS spectra of Cs3d, Ag3d, Bi4f, and Br3p core levels were fitted.

The calculated atomic ratios of the $Cs_2AgBiBr_6$ powders can be determined to be a 2:1:1:6 ratio of Cs:Ag:Bi:Br. This stoichiometric ratio of Br has been demonstrated important to stabilize the $Cs_2AgBiBr_6$ electronic structure.

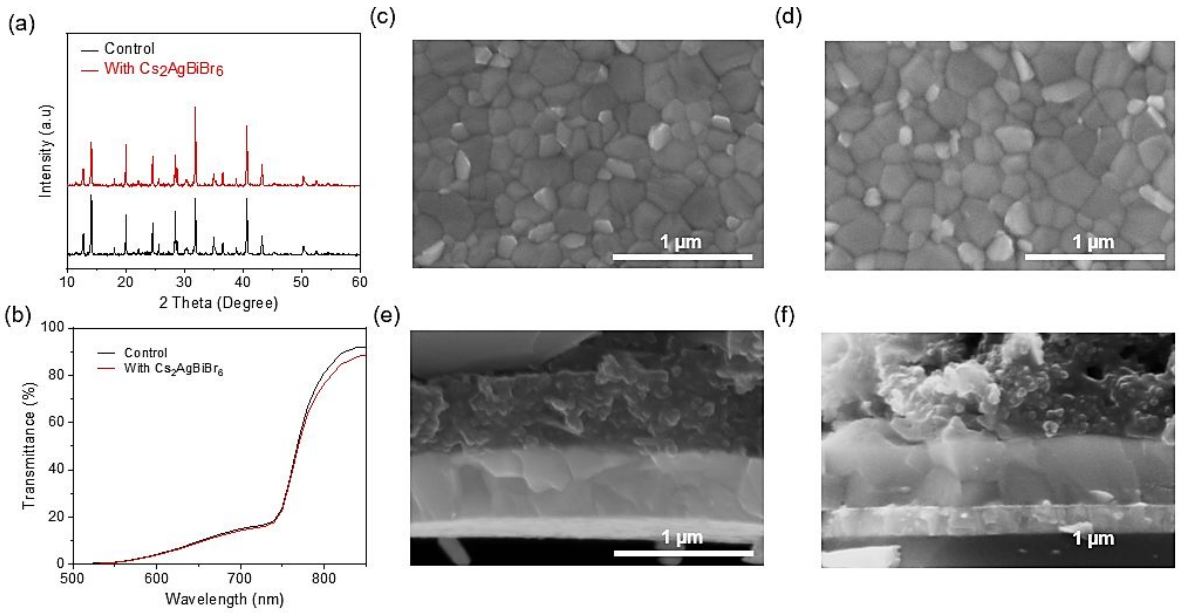

Figure 3. (a) XRD patterns and (b) transmittance curves of control and $Cs_2AgBiBr_6$-treated perovskite films. Surface SEM images of perovskite films deposited on ITO/SnO_2 (c) without and (d) with $Cs_2AgBiBr_6$ treatment. Cross-section SEM images of (e) control and (f) $Cs_2AgBiBr_6$-treated PSCs.

The double perovskite solutions with various concentrations from 0 to 5 mg/ml were introduced to the triple cation single perovskite by spin coating. The XRD spectra of the pristine (control) single perovskite and the $Cs_2AgBiBr_6$-treated single perovskite film are determined to be almost identical (Fig. 3a), suggesting that the diffraction peak of double perovskite nanocrystals is weak to be detected. Additionally, the characteristic XRD peak of PbI_2 (2theta ~ 12.7 deg.) was suppressed in $Cs_2AgBiBr_6$-treated film. Fig. S1 shows the intensity of the perovskite peak as a function of time, in which the $Cs_2AgBiBr_6$-treated film displayed a slower degradation rate, providing further evidence for the passivation effect. The light transmittance spectra for both the control and $Cs_2AgBiBr_6$-treated single perovskite film have been recorded as shown in Fig. 3b, where the deposited $Cs_2AgBiBr_6$ layer did not affect the absorption of single perovskite

due to the limited absorption of $Cs_2AgBiBr_6$ at long wavelengths as shown in Fig. 1d. The top-view scanning electron microscopy (SEM) images for perovskite films deposited on the SnO_2-coated indium tin oxide (ITO) substrate without and with $Cs_2AgBiBr_6$ treatment are shown in Fig. 3c and Fig. 3d, respectively. It showed that the double perovskite passivation layer suppressed the decomposition of PbI_2. Through the cross-sectional SEM images of Glass/ITO/SnO_2/perovskite/Spiro-OMeTAD/Au PSCs without and with $Cs_2AgBiBr_6$ treatment (Fig. 3e and Fig. 3f, respectively) it is demonstrated that the coated thin double perovskite $Cs_2AgBiBr_6$ layer did not impact the single perovskite layer thickness remarkably.

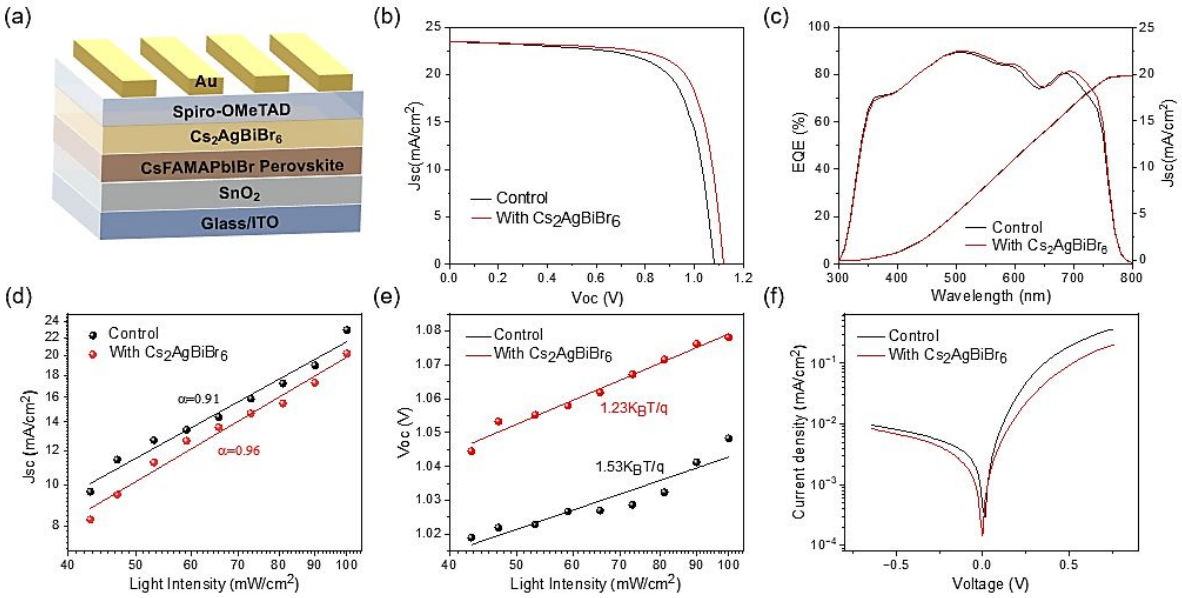

Figure 4. (a) Schematic diagram of the PSC. (b) ME curves and (c) EQE with integrated current spectra of control and $Cs_2AgBiBr_6$-treated PSCs. The fitting curves of the J_{SC} (d) and (e) under different illuminated light intensities for control and $Cs_2AgBiBr_6$-treated devices. (f) Dark J–V curves of control and $Cs_2AgBiBr_6$-treated PSCs.

The schematic diagram of the devices with n-i-p architecture Glass/ITO/SnO_2/Perovskite/Spiro-OMeTAD/Au is shown in Fig. 4a. The band gap alignment can be found in Fig. S2. The current density-voltage (J-V) curves of champion control and $Cs_2AgBiBr_6$ treated PSCs were presented in Fig. 4b. The $Cs_2AgBiBr_6$ treated PSC exhibited a comparable .while a substantial enhancement in . The increased

was attributed to the passivation effect of the $CS_2AgBiBr_6$ layer, leading to less nonradiative recombination between the perovskite and HTL. Fig. S3 presents J-V evidence indicating that the optimal concentration of $Cs_2AgBiBr_6$ is 1 mg/ml. EQE spectra indicate that the double perovskite layer did not impact the photon conversion to electron, and the integrated photocurrent densities in EQE are ~ 20 mA/cm^2 for both devices, which is slightly lower than those derived from *J-V* curves because the cells for EQE measurement-do not have pre-conditioning, e.g., light soaking.

The relationship of light intensity with and was studied to investigate the effect of $Cs_2AgBiBr_6$ treatment on charge carrier transport and recombination in PSCs. The and light intensity confirms a power-law behavior: [35]

=

In which J_{SC} is the short-circuit current density under different light intensities, is the light intensity and is the ideality factor of . As plotted in Fig. 4d, the □value for the PSC with and without the $Cs_2AgBiBr_6$ interlayer were 0.96 and 0.91, respectively. The increased □value of the $Cs_2AgBiBr_6$-treated PSC indicates a more efficient charge extraction capability. The ideality factor *n* of values under different light intensities can be obtained as below: [35]

= +——

Where is the open-circuit voltage under different light intensities, is the open-circuit voltage under standard light intensity, is the ideality factor, is the Boltzmann constant, is the temperature, is the electron charge and is the light intensity. As shown in Fig. 4e, we found the $Cs_2AgBiBr_6$-treated PSC showed a smaller slope of 1.23 / compared with the control device with a slope of 1.53 / , suggesting that the introduction of the double perovskite interlayer suppressed the charge recombination as well as the intrinsic defect density. Fig. 4f shows the dark *J–V* curves of control and $Cs_2AgBiBr_6$-treated devices. The current density of PSC with $Cs_2AgBiBr_6$ interlayer was lower than that of the control device in the dark, demonstrating a lower leakage due to the efficient collection of photo-generated charge carriers

through the charge transfer layer. This indicates that the $Cs_2AgBiBr_6$ double perovskite layer suppressed the recombination of photo-generated charge carriers.

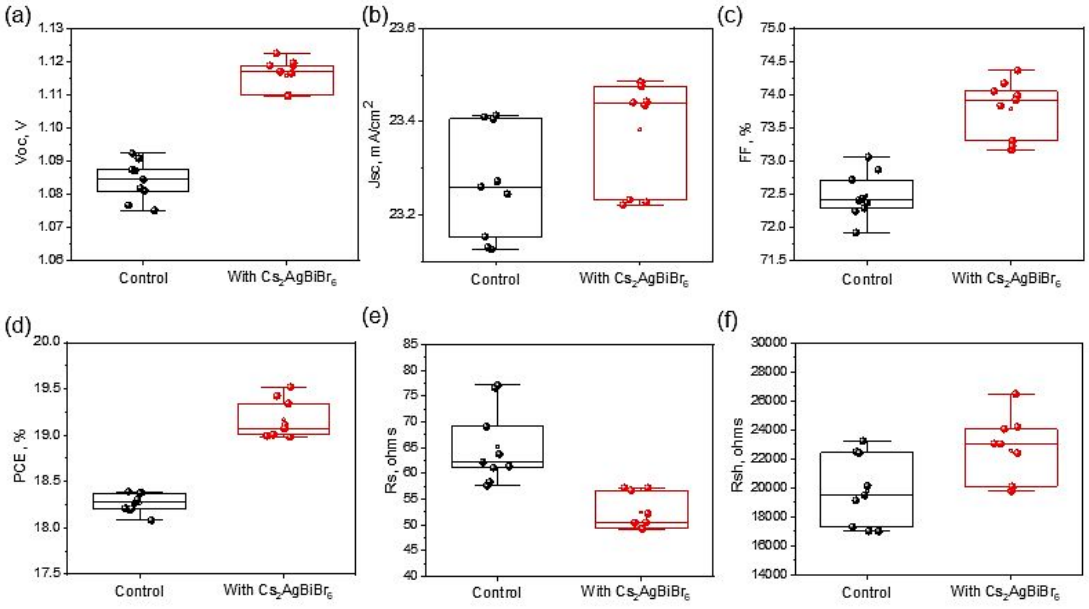

Figure 5. Statistical distribution of (a) open-circuit voltage (V_{OC}), (b) short-circuit current density (J_{SC}), (c) fill factor (FF), (d) power conversion efficiency (PCE), (e) series resistance (Rs) and (f) shunt resistance (Rsh) of devices without and with different concentrations of $Cs_2AgBiBr_6$.

The device performance statistical distribution is shown in Fig. 5. The control PSC showed a decent champion PCE of 18.39%, with a of 1.09 V, a of 23.40 mA/cm^2, and an FF of 73.06%. Following $CS_2AgBiBr_6$ treatment, the champion device achieved a significantly enhanced PCE of 19.52%, accompanied with a of 1.12V, a of 23.48 mA/cm^2 and an FF of 74.36%. The observed boost in , FF and PCE provided evidence of the effective passivation impact attributed to the $Cs_2AgBiBr_6$ layer at the perovskite/HTL interface. In Fig S4, , FF and PCE increased with rising concentration from 0 mg/ml to 1mg/ml, while further elevating the concentration beyond 1 mg/ml resulted in a decline in performance. The displayed a contrasting trend, however, it remains superior to the control PSC. The reduction in Rs and the enhancement in Rsh are outcomes of optimized contacts and minimized defects within the solar cell.

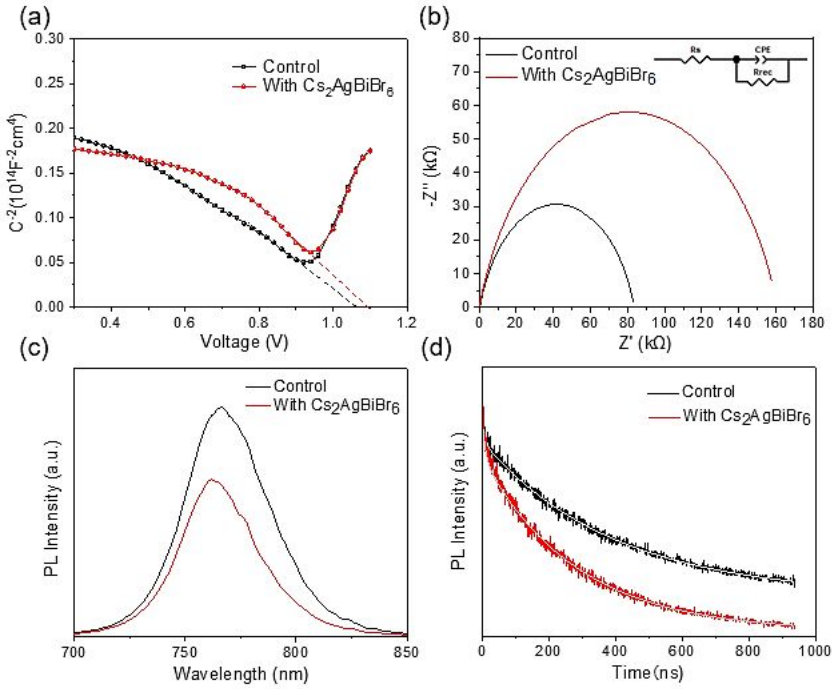

Figure 6. (a) Mott–Schottky plots and (b) Nyquist plots of the control and $Cs_2AgBiBr_6$-treated PSCs. Steady state PL (c) and TRPL spectra (d) of control with the structures of ITO/SnO_2/perovskite and treated PSCs with the structures of ITO/SnO2/perovskite/$Cs_2AgBiBr_6$.

Figure 6a indicated a C^{M}-V plot, also known as Mott–Schottky plot. The built-in voltage ( ) of PSCs, related to the depletion region length, can be extrapolated from the plots.[36] As illustrated in Fig. 6a, the obtained of the $Cs_2AgBiBr_6$-treated PSC is higher than that of the control PSC, which can be attributed to the lower charge accumulation at the perovskite/$Cs_2AgBiBr_6$ interface. EIS was conducted to analyze the recombination resistance in the PSCs. The EIS spectra of the cells and the equivalent circuit model are displayed in Fig. 6b, in which is series resistance, is recombination resistance, and CPE is capacitance. The $Cs_2AgBiBr_6$-treated PSC demonstrated a significantly higher value of 1.6×10^5 P□in contrast to the control device with a value of 8.3×10^4 P□The results indicated that the double perovskite interlayer served as a passivation layer, inhibiting undesired charge carrier recombination and enhancing

the electron extraction. [37] The steady-state photoluminescence (PL) and time-resolved photoluminescence (TRPL) spectra are shown in Fig. 6c, d. The perovskite film was deposited on the ITO/SnO_2 substrate. The PL intensity of $Cs_2AgBiBr_6$ treated films in Fig.6c was noticeably reduced compared with pristine films, suggesting an effective electron extraction at perovskite/ETL interface. Additionally, the PL peak presented a blue-shift from 766 nm to 763 nm, demonstrating a lower electron trap-state density for the $Cs_2AgBiBr_6$ treated perovskite. [38] The TRPL spectrum reveals the fast decay component $_1$, which is ascribed to trap-assisted nonradiative recombination, and a slow decay component $_2$ associating with radiative recombination of free carriers. [39] The $Cs_2AgBiBr_6$ treated sample exhibits a lifetimes Q□oI R□ which is shorter than the lifetime 7 6R□ of the pristine sample. This shorter lifetime indicates the enhanced efficiency in electron extraction at the ETL/perovskite interface, aligning with the observations in the steady-state PL spectra.

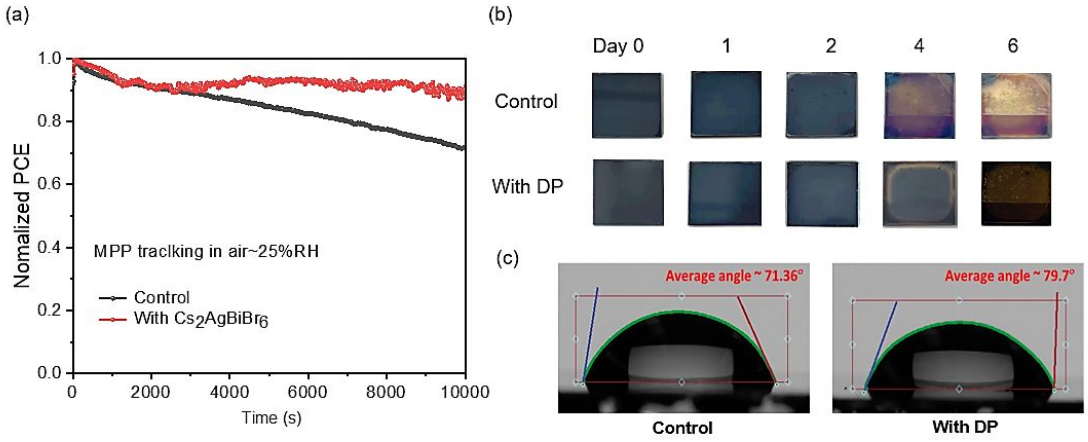

Figure 7. (a) Stability of unencapsulated control and $Cs_2AgBiBr_6$-treated PSCs for 7 days in air with RH 25%. (b) Photographic images of the color changes of the perovskite films in ambient over time. (c) The contact angle of the control and $Cs_2AgBiBr_6$-treated films.

The device stability was analyzed through maximum power point (MPP) tracking, as depicted in Figure 7a. All the devices were unencapsulated and tested in ambient with humidity ~25% RH for 7 days. The $Cs_2AgBiBr_6$ treated PSC retained 89.4% of the initial PCE after 10000s, whereas only 71.9% of the initial PCE could be retained for the control PSC. This behavior indicates that the double perovskite passivate layer may limit the halide ions migration into the hole transport layer. Fig.7b provides additional evidence. The color change in the control film became apparent after 2 days, whereas the $Cs_2AgBiBr_6$-treated film started to degrade after 4 days, as illustrated in the photographic images in ambient conditions over time. The improved stability with $Cs_2AgBiBr_6$ treatment is ascribed to two factors: 1) effective passivation of defects, such as the passivation of grain boundary and 2) the $Cs_2AgBiBr_6$ capping layer blocked the moisture into the perovskite layer, which is evidenced by the enhanced surface hydrophobicity, as confirmed by water contact angles (Fig. 7c).

4. Conclusion

We have demonstrated the effectiveness of incorporating a double perovskite $Cs_2AgBiBr_6$ capping layer onto single perovskite solar cells (PSCs), resulting in simultaneous enhancements in device efficiency and stability. The $Cs_2AgBiBr_6$ interlayer plays a multifaceted role by mitigating nonradiative recombination, passivating surface defects within the single perovskite layer, and facilitating exciton transportation. Through optimization, the $Cs_2AgBiBr_6$-treated PSCs exhibited a noticeable increase in Voc alongside a superior power conversion efficiency (PCE) of 19.52%, while also demonstrating enhanced stability under ambient conditions. Our findings highlight the efficacy of utilizing a double perovskite passivation layer as a viable strategy for augmenting the performance of low-cost, easily fabricable, high-efficiency perovskite solar cells. This approach holds significant promise in expediting the commercialization of PSCs, thus contributing to the advancement of renewable energy technologies.

Conflict of Interests

There are no conflicts to declare.

Acknowledgment

This work is supported by the Department of Energy, Energy Efficiency and Renewable Energy under Award DE-EE0009833, National Science Foundation under contract No. DMR-2127640 and DMR 2127630, and TI- 2329871. The work was also partially supported by the U.S. Department of Energy under Contract No. DE-AC36-08GO28308 with Alliance for Sustainable Energy, Limited Liability Company (LLC), the Manager and Operator of the National Renewable Energy Laboratory. We acknowledge the support from the Advanced Perovskite Cells and Modules program of the National Center for Photovoltaics, funded by the U.S. Department of Energy, Office of Energy Efficiency and Renewable Energy, Solar Energy Technologies Office. The views expressed in the article do not necessarily represent the views of the DOE or the U.S. Government.

Reference

(1)Kim, H.-S., Lee, C.-R., Im, J.-H., Lee, K.-B., Moehl, T., Marchioro, A., Moon, S.-J., Humphry-Baker, R., Yum, J.-H., Moser, J.E., Lead iodide perovskite sensitized all-solid-state submicron thin film mesoscopic solar cell with efficiency exceeding 9%, Scientific reports, (2012)2 591.
(2)Xing, G., Mathews, N., Sun, S., Lim, S.S., Lam, Y.M., Grätzel, M., Mhaisalkar, S., Sum, T.C., Long-range balanced electron-and hole-transport lengths in organic-inorganic CH3NH3PbI3, Science, (2013)342 344-347.
(3)Kim, M., Kim, G.-H., Lee, T.K., Choi, I.W., Choi, H.W., Jo, Y., Yoon, Y.J., Kim, J.W., Lee, J., Huh, D., Methylammonium chloride induces intermediate phase stabilization for efficient perovskite solar cells, Joule, (2019)3 2179-2192.
(4)Yoo, J.J., Seo, G., Chua, M.R., Park, T.G., Lu, Y., Rotermund, F., Kim, Y.K., Moon, C.S., Jeon, N.J., Correa-Baena, J.P., Bulovic, V., Shin, S.S., Bawendi, M.G., Seo, J., Efficient perovskite solar cells via improved carrier management, Nature, (2021)590 587-593.
(5)Bi, D., Yi, C., Luo, J., Décoppet, J.-D., Zhang, F., Zakeeruddin, S.M., Li, X., Hagfeldt, A., Grätzel, M., Polymer-templated nucleation and crystal growth of perovskite films for solar cells with efficiency greater than 21%, Nature Energy, (2016)1 1-5.

(6)Kojima, A., Teshima, K., Shirai, Y., Miyasaka, T., Organometal halide perovskites as visible-light sensitizers for photovoltaic cells, Journal of the american chemical society, (2009)131 6050-6051.
(7)Min, H., Lee, D.Y., Kim, J., Kim, G., Lee, K.S., Kim, J., Paik, M.J., Kim, Y.K., Kim, K.S., Kim, M.G., Shin, T.J., Il Seok, S., Perovskite solar cells with atomically coherent interlayers on SnO2 electrodes, Nature, (2021)598 444-450.
(8), National Renewable Energy Laboratory Best Research-Cell Efficiency chart.
(9)Miyasaka, T., Kulkarni, A., Kim, G.M., Öz, S., Jena, A.K., Perovskite solar cells: can we go organic□free, lead□free, and dopant□free?, Advanced Energy Materials, (2020)10 1902500.
(10)Chen, S., Xiao, X., Gu, H., Huang, J., Iodine reduction for reproducible and high-performance perovskite solar cells and modules, Sci Adv, (2021)7 eabe8130.
(11)Motti, S.G., Meggiolaro, D., Martani, S., Sorrentino, R., Barker, A.J., De Angelis, F., Petrozza, A., Defect Activity in Lead Halide Perovskites, Adv Mater, (2019)31 e1901183.
(12)Han, T.H., Tan, S., Xue, J., Meng, L., Lee, J.W., Yang, Y., Interface and Defect Engineering for Metal Halide Perovskite Optoelectronic Devices, Adv Mater, (2019)31 e1803515.
(13)Jang, Y.-W., Lee, S., Yeom, K.M., Jeong, K., Choi, K., Choi, M., Noh, J.H., Intact 2D/3D halide junction perovskite solar cells via solid-phase in-plane growth, Nature Energy, (2021)6 63-71.
(14)Turren-Cruz, S.H., Hagfeldt, A., Saliba, M., Methylammonium-free, high-performance, and stable perovskite solar cells on a planar architecture, Science, (2018)362 449-453.
(15)Kim, M., Motti, S.G., Sorrentino, R., Petrozza, A., Enhanced solar cell stability by hygroscopic polymer passivation of metal halide perovskite thin film, Energy & Environmental Science, (2018)11 2609-2619.
(16)Jung, E.H., Jeon, N.J., Park, E.Y., Moon, C.S., Shin, T.J., Yang, T.-Y., Noh, J.H., Seo, J., Efficient, stable and scalable perovskite solar cells using poly (3-hexylthiophene), Nature, (2019)567 511-515.
(17)Wang, R., Xue, J., Wang, K.L., Wang, Z.K., Luo, Y., Fenning, D., Xu, G., Nuryyeva, S., Huang, T., Zhao, Y., Yang, J.L., Zhu, J., Wang, M., Tan, S., Yavuz, I., Houk, K.N., Yang, Y., Constructive molecular configurations for surface-defect passivation of perovskite photovoltaics, Science, (2019)366 1509-1513.
(18)Bai, S., Da, P., Li, C., Wang, Z., Yuan, Z., Fu, F., Kawecki, M., Liu, X., Sakai, N., Wang, J.T.-W., Planar perovskite solar cells with long-term stability using ionic liquid additives, Nature, (2019)571 245-250.
(19)Li, M., Zhao, C., Wang, Z.K., Zhang, C.C., Lee, H.K., Pockett, A., Barbé, J., Tsoi, W.C., Yang, Y.G., Carnie, M.J., Interface modification by ionic liquid: a promising candidate for indoor light harvesting and stability improvement of planar perovskite solar cells, Advanced Energy Materials, (2018)8 1801509.
(20)Yoo, J.J., Wieghold, S., Sponseller, M.C., Chua, M.R., Bertram, S.N., Hartono, N.T.P., Tresback, J.S., Hansen, E.C., Correa-Baena, J.-P., □X□ V., An interface stabilized perovskite solar cell with high stabilized efficiency and low voltage loss, Energy & Environmental Science, (2019)12 2192-2199.
(21)O'Keeffe, P., Catone, D., Paladini, A., Toschi, F., Turchini, S., Avaldi, L., Martelli, F., Agresti, A., Pescetelli, S., Del Rio Castillo, A.E., Bonaccorso, F., Di Carlo, A., Graphene-Induced Improvements of Perovskite Solar Cell Stability: Effects on Hot-Carriers, Nano Lett, (2019)19 684-691.
(22)Cho, Y., Soufiani, A.M., Yun, J.S., Kim, J., Lee, D.S., Seidel, J., Deng, X., Green, M.A., Huang, S., Ho□Baillie, A.W., Mixed 3D–2D passivation treatment for mixed□cation lead mixed□halide perovskite solar cells for higher efficiency and better stability, Advanced Energy Materials, (2018)8 1703392.
(23)Igbari, F., Wang, Z.K., Liao, L.S., Progress of lead□free halide double perovskites, Advanced Energy Materials, (2019)9 1803150.
(24)Zhang, Z., Liang, Y., Huang, H., Liu, X., Li, Q., Chen, L., Xu, D., Stable and highly efficient photocatalysis with lead□free double□perovskite of Cs2AgBiBr6, Angewandte Chemie International Edition, (2019)58 7263-7267.
(25)Wu, C., Du, B., Luo, W., Liu, Y., Li, T., Wang, D., Guo, X., Ting, H., Fang, Z., Wang, S., Highly efficient and stable self□powered ultraviolet and deep□blue photodetector based on Cs2AgBiBr6/SnO2 heterojunction, Advanced Optical Materials, (2018)6 1800811.

(26)Wu, C., Zhang, Q., Liu, Y., Luo, W., Guo, X., Huang, Z., Ting, H., Sun, W., Zhong, X., Wei, S., Wang, S., Chen, Z., Xiao, L., The Dawn of Lead-Free Perovskite Solar Cell: Highly Stable Double Perovskite Cs2AgBiBr6 Film, Adv Sci (Weinh), (2018)5 1700759.
(27)Igbari, F., Wang, R., Wang, Z.K., Ma, X.J., Wang, Q., Wang, K.L., Zhang, Y., Liao, L.S., Yang, Y., Composition Stoichiometry of Cs2AgBiBr6 Films for Highly Efficient Lead-Free Perovskite Solar Cells, Nano Lett, (2019)19 2066-2073.
(28)Zhang, Z., Sun, Q., Lu, Y., Lu, F., Mu, X., Wei, S.-H., Sui, M., Hydrogenated Cs2AgBiBr6 for significantly improved efficiency of lead-free inorganic double perovskite solar cell, Nature communications, (2022)13 3397.
(29)Chowdhury, T.A., Zafar, M.A.B., Islam, M.S.-U., Shahinuzzaman, M., Islam, M.A., Khandaker, M.U., Stability of perovskite solar cells: issues and prospects, RSC Advances, (2023)13 1787-1810.
(30)Christians, J.A., Zhang, F., Bramante, R.C., Reese, M.O., Schloemer, T.H., Sellinger, A., van Hest, M.F., Zhu, K., Berry, J.J., Luther, J.M., Stability at scale: challenges of module interconnects for perovskite photovoltaics, ACS Energy Letters, (2018)3 2502-2503.
(31)Zheng, K., Pullerits, T.n., Two dimensions are better for perovskites, ACS Publications, 2019, pp. 5881-5885.
(32)Zhang, Z., Zhang, Y., Guo, X., Wang, D., Lao, Y., Qu, B., Xiao, L., Chen, Z., Realizing high-efficiency and stable perovskite solar cells via double-perovskite nanocrystal passivation, ACS Applied Energy Materials, (2022)5 1169-1174.
(33)Vijayaraghavan, S., Wall, J., Menon, H.G., Duan, X., Guo, L., Amin, A., Han, X., Kong, L., Zheng, Y., Li, L., Interfacial engineering with NiOx nanofibers as hole transport layer for carbon-based perovskite solar cells, Solar Energy, (2021)230 591-597.
(34)Slavney, A.H., Hu, T., Lindenberg, A.M., Karunadasa, H.I., A bismuth-halide double perovskite with long carrier recombination lifetime for photovoltaic applications, Journal of the American chemical society, (2016)138 2138-2141.
(35)Su, Y., Yang, J., Liu, G., Sheng, W., Zhang, J., Zhong, Y., Tan, L., Chen, Y., Acetic Acid□Assisted Synergistic Modulation of Crystallization Kinetics and Inhibition of Sn2+ Oxidation in Tin□Based Perovskite Solar Cells, Advanced Functional Materials, (2022)32 2109631.
(36)Yang, G., Wang, C., Lei, H., Zheng, X., Qin, P., Xiong, L., Zhao, X., Yan, Y., Fang, G., Interface engineering in planar perovskite solar cells: energy level alignment, perovskite morphology control and high performance achievement, Journal of Materials Chemistry A, (2017)5 1658-1666.
(37)Yang, C., Wang, H., Miao, Y., Chen, C., Zhai, M., Bao, Q., Ding, X., Yang, X., Cheng, M., Interfacial molecular doping and energy level alignment regulation for perovskite solar cells with efficiency exceeding 23%, ACS Energy Letters, (2021)6 2690-2696.
(38)Shao, Y., Xiao, Z., Bi, C., Yuan, Y., Huang, J., Origin and elimination of photocurrent hysteresis by fullerene passivation in CH3NH3PbI3 planar heterojunction solar cells, Nature communications, (2014)5 5784.
(39)Wu, Z., Jiang, M., Liu, Z., Jamshaid, A., Ono, L.K., Qi, Y., Highly efficient perovskite solar cells enabled by multiple ligand passivation, Advanced Energy Materials, (2020)10 1903696.